Deciphering the Origin of High-Order Periodic and Aperiodic Cyclic Voltammetric Responses During Oxidation Processes on Platinum

Hamilton Varela[†] and Katharina Krischer*[,†,‡]

Fritz-Haber-Institut der Max-Planck-Gesellschaft, Faradayweg 4−6, D-14195 Berlin, Germany, and Physik-Department E19, Technische Universität München, James-Franck-Strasse 1, D-85748 Garching, Germany

Received: August 2, 2002; In Final Form: September 27, 2002

We report cyclic voltammograms of the hydrogen electrooxidation reaction on a rotating Pt ring electrode in diluted electrolytes that are either aperiodic or possess a period which is a multiple of the period of the cycling voltage. The complex voltammetric responses are experimentally studied in two electrolytes with different compositions of the base electrolyte (and thus different conductivity) as a function of the positive turning point of the applied voltage. The behavior can be rationalized in terms of the interaction between the inhibition of H_2 oxidation by Pt−oxides, the roughening of the electrode due to oxide reduction and its subsequent smoothing as well as a nonnegligible uncompensated voltage drop through the electrolyte. The proposed mechanism is translated into a mathematical model consisting of a set of four ordinary differential equations. The model indeed captures the main experimental findings. Since the principle ideas do not depend on the specific kinetics of the oxidation reaction under investigation, the mechanism should be operative in a variety of electrochemical systems. In particular, we suggest that it may underlie the complex cyclic voltammograms observed during many oxidation reactions of small organic molecules.

1. Introduction

Cyclic voltammetry is one of the simplest and most widespread techniques for investigations of electrochemical reactions.[1,2] In a conventional cyclic voltammetric experiment, the potential difference between the working (WE) and the reference (RE) electrodes is externally varied by means of a potentiostat and the potential range between two turning points is repeatedly visited on a linear time scale. The curve showing the measured current as a function of the applied potential difference is called a cyclic voltammogram (CV).

A CV usually begins to repeat itself after a finite number of voltage cycles; i.e., it settles down to a stationary profile invariant in time. Thus, the current time trace is periodic and possesses the same period as the imposed voltage scan. This conventional response represents a so-called "period-1 CV".

A high-order periodic CV is a CV in which the period of the current response is a multiple of the period of the applied voltage. For example, in a period-2 CV, the current time trace repeats itself after two periods of the external voltage. Such high-order periodic CVs as well as aperiodic CVs, in which the current never settles down to a periodic behavior, were reported by Schell and co-workers for the oxidation of several organic molecules, such as methanol, ethanol, and propanol, on Pt and Pd electrodes in both acidic and alkaline media.[3−10] The complex voltammetric responses were obtained within a certain range of the positive turning point of the applied voltage over wide ranges of other control parameters, such as concentrations of the educts, electrolyte conductivity, or rotation rate of the electrode. Another example of such complex voltammetric behavior has recently been observed by Dolata and Kawcznski[11] during the anodic dissolution of copper in concentrated sulfuric acid.

Schell and co-workers suggest that a nonlinear feedback mechanism, which involves the reaction of PtOH with the intermediate PtCO as well as the conversion of PtOH to Pt−oxides, is crucial for the occurrence of complex voltammetric responses. The unusual cyclic voltammetric behavior is then believed to be the result of the interplay between the periodically forced applied potential (i.e., the potential cycling) and the for each organic compound specific nonlinearities of the electrochemical reaction.[7,8]

Recently, we reported very similar phenomena during hydrogen oxidation on a rotating Pt ring electrode in an acidic electrolyte of low ionic strength.[12] In this system we can a priori exclude that any carbon containing intermediate is essential for the mechanism causing the complex voltammetric behavior. In the present contribution, we suggest a general mechanism for the occurrence of the high-order periodic and aperiodic cyclic voltammograms. The mechanism only depends on properties of the electrode material (Pt and Pd) but is independent of the specific oxidation reactions under investigation. It thus should hold for both the hydrogen oxidation reaction and the oxidation of organic substances.

The paper is structured as follows: After introducing our experimental setup (section 2.1), we present further experimental results on complex cyclic voltammetry during hydrogen oxidation on Pt electrodes (section 2.2). In section 2.3, those features of the experimental CVs are highlighted which form the basis of our explanation of the complex voltammetric responses. In sections 3.1 and 3.2, the mechanism is translated into a mathematical model and simulations are presented, respectively. The discussion in section 4 focuses on a comparison between

* Corresponding author. E-mail: krischer@ph.tum.de Telephone: (+ 49 89) 289 12535. Fax: (+ 49 89) 289 12530.
[†] Fritz-Haber-Institut der Max-Planck-Gesellschaft.
[‡] Technische Universität München.

10.1021/jp026673g CCC: $22.00
Published on Web 11/06/2002

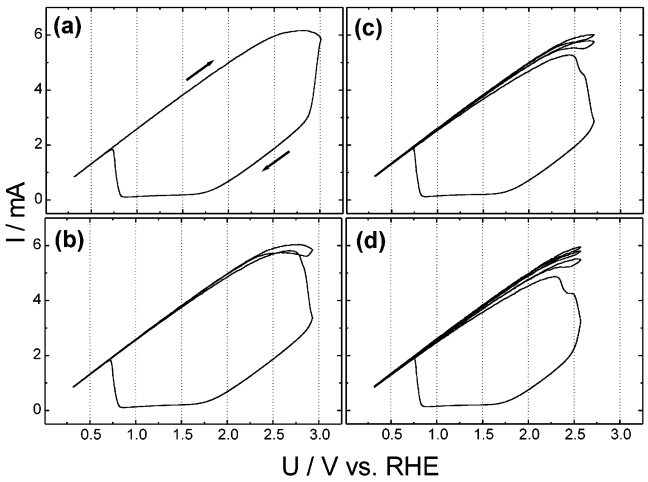

Figure 1. Cyclic voltammograms of Pt|H_2SO_4|H_2 at different positive turning points of the external voltage (U_2): (a) 3.01, (b) 2.93, (c) 2.71, and (d) 2.57 V. Remaining parameters: negative turning point U_1 = 0.31 V; scan rate 0.1 V s^{-1}; electrolyte, 0.875 mM H_2SO_4, H_2-saturated; uncompensated resistance, 410 ± 5 Ω; rotation rate of the WE, 20 Hz. The anodic turning point was decreased stepwise, i.e., the order of measurements is a−d.

simulations and experimental results. Finally, the main findings are summarized in the concluding section, section 5.

2. Experiments

2.1. Experimental Setup. A rotating Pt ring (outer diameter 30 mm, width 1 mm) embedded into a Teflon cylinder served as working electrode (WE). The reference electrode and the counter electrode were a Hg/Hg_2SO_4 electrode and a Pt ring electrode, respectively. The electrochemical cell and the arrangement of the electrodes are described in detail in refs 12 and 13. In all experiments shown, the WE was rotated at 20 Hz and the applied voltage was scanned with 100 mV s^{-1}. All potentials are given with respect to the reversible hydrogen electrode (RHE). The potentiostat used was built by the Electronic Laboratory, Fritz-Haber-Institut der MPG, Berlin, Germany.

The supporting electrolyte, diluted H_2SO_4, was prepared from concentrated H_2SO_4 (Merck, p.a. grade) and Millipore water (Millipore Milli-Q water, 18 MΩ cm). H_2 (5 N, Linde) was bubbled continuously through the solution during the experiments. Below we refer to this system as the Pt|H_2SO_4|H_2 system.

The Pt-ring working electrode was polished to a mirror finish with acetone based fine diamond paste (Ernst Winter) down to a particle size of 0.25 μm, washed with high purity water, and then additionally cleaned with pure water under an ultrasonic bath a few times. Before each experiment, the working electrode was electrochemically annealed,[14] i.e., cycled under N_2 between 0.05 and 1.4 V vs RHE at 0.1 V s^{-1} for 1 h, and then maintained in open circuit potential in the same solution for 30 min during H_2 saturation.

2.2. Results. Figure 1 shows four CVs of the Pt|H_2SO_4|H_2 system which were obtained for four different values of the positive turning point (U_2) and otherwise identical experimental conditions. The current/voltage curve depicted in Figure 1a was obtained for the most positive value of U_2 and can be easily rationalized.

Hydrogen electrooxidation is known to proceed through the following steps:[2] (i) diffusion of H_2 from the bulk electrolyte to the electrode surface, (ii) dissociative adsorption of surface H_2 onto bare Pt sites, and (iii) electrochemical oxidation of adsorbed hydrogen atoms accompanied by hydration

$$H_2^{bulk} \rightarrow H_2^{surface} \quad \text{(i)}$$

$$2Pt + H_2^{surface} \rightarrow 2Pt{-}H \quad \text{(ii)}$$

$$Pt{-}H + H_2O \rightarrow H_3O^+ + e^- + Pt \quad \text{(iii)}$$

The initial linear increase of the current, I, with increasing applied potential, U, reflects the high electrolyte resistance, which determines the form of the I/U curve at low overpotential. The potential-independent current plateau at larger values of U indicates mass transport limitation (step i). The current decrease close to the positive turning point is due to the oxidation of the Pt surface according to steps iv and v[15,16] since the dissociation rate of H_2 (step ii) is negligible on PtO(H).

$$Pt + H_2O \rightarrow Pt{-}OH + H^+ + e^- \quad \text{(iv)}$$

$$Pt{-}OH \rightarrow Pt{-}O + H^+ + e^- \quad \text{(v)}$$

For this comparatively high electrolyte resistance of the experiments, the decrease in current density leads to an increase in the true electrode potential which becomes close to the positive turning point so positive that oxygen evolution occurs. Hence, the linearly decreasing current on the negative scan results from oxygen evolution. Once Pt−oxide (step v) is formed the reverse processes of steps iv and v occur at much higher (negative) overpotential, causing the large hysteresis between on the forward and backward scans in the CV.

Upon decreasing U_2, one would intuitively expect that, from a threshold potential on, hydrogen is oxidized on the forward and backward scans with approximately the same rates since the potential at which Pt is oxidized is not reached anymore. However, this behavior is only found for considerably lower values of U_2. For intermediate values of U_2, high-order periodic CVs are observed which are composed of a different number of these two limiting CVs. Examples of period-2, 3, and 4 CVs, which emerged after decreasing U_2 in steps of 20 mV, are shown in Figure 1b−d. For simplicity, in the following, we will denote a current−voltage cycle in which the H_2 oxidation current remains high throughout the cycle and thus exhibits around the positive turning point only a small hysteresis as an S cycle and one during which oxide formation takes place leading to a large hysteresis in the oxidation current as an L cycle. In the period-2 CV (Figure 1b), S and L cycles alternate; we term such a period-2 response an SL state. In Figure 1, parts c and d, two and three S cycles, respectively, are periodically followed by an L cycle. These complex CVs are thus examples of period-3 S^2L and period-4 S^3L states.

A closer examination of the S cycles in Figure 1, parts c and d, shows that they are not identical but differ slightly in the maximal current density close to U_2. When plotting the current as a function of time, as done in Figure 2b for the S^3L state of Figure 1d, it becomes apparent that the maximum current decreases for successive S cycles (cycles 1−3), is minimal for an L cycle (cycle 4). It is reset to its maximal value for the first S cycle after an L cycle (cycle 5), from where the slow decrease starts again. Note that in Figure 2 and all successive figures time has been normalized to the period of a voltage cycle, T_u. Figure 2a shows for clarity the externally imposed voltage, U, as a function of time.

Since we are working under potential control and in an electrolyte with low ionic strength, lower values of the current density imply that the true electrode potential, ϕ_{DL}, takes on

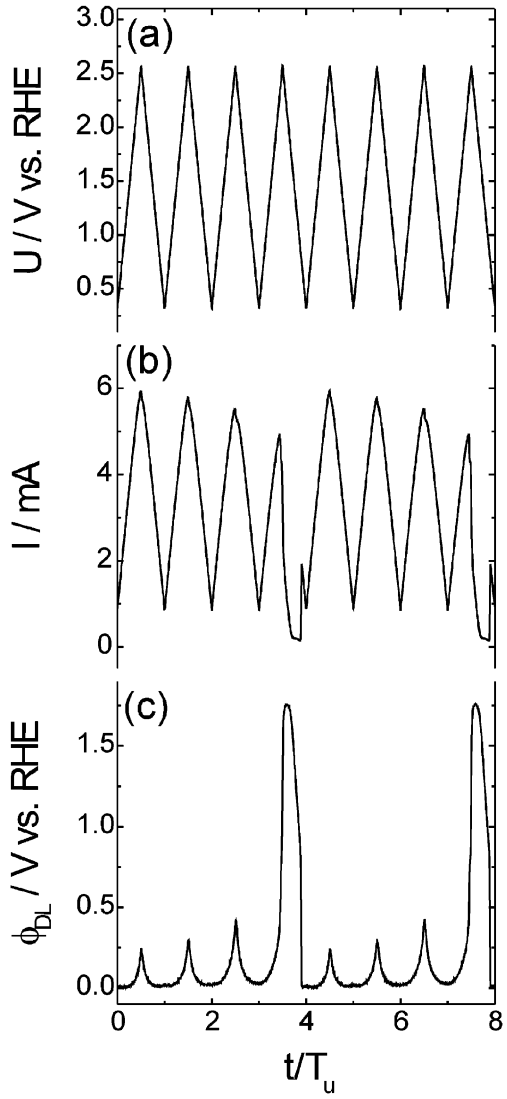

Figure 2. (a) Externally applied voltage, U, (b) current, I, and (c) true electrode potential, ϕ_{DL}, as a function of time (measured in units of the period of the applied voltage T_u) for the period-4 CV shown in Figure 1d. (ϕ_{DL} was calculated according to $U = \phi_{DL} - R_\Omega I$, for R_Ω = 410 Ω.)

larger values. Thus, although U_2 is kept constant during the cycling, the upper limit of the true electrode potential, $\phi_{DL,max}$, differs in the individual cycles of a high-order periodic CV. This can be seen in Figure 2c, in which ϕ_{DL} is plotted vs time. ϕ_{DL} was calculated from $U - IR_\Omega = \phi_{DL}$, where R_Ω is the uncompensated cell resistance.

Owing to the drastic differences of $\phi_{DL,max}$ for an S and an L cycle as well as its distinct values for each S cycle within one full period of the CV, we use $\phi_{DL,max}$ as variable for the further characterization of the complex voltammetric responses. In the bifurcation diagram depicted in Figure 3 $\phi_{DL,max}$ values are plotted against the value of the positive turning point, U_2, which was decreased from 3.03 V in steps of 20 mV. Up to U_2=2.95 V only period-1 CVs with large hysteresis cycles (L cycles) existed. In an L cycle, $\phi_{DL,max}$ takes on a value of about 1.82 V (squares in Figure 3). When the U_2 value is further decreased the period two response appears at U_2 = 2.93 V giving rise to another branch of $\phi_{DL,max}$ (circles in Figure 3). The coexistence of these two branches evidences period-2 SL responses like the one shown in Figure 1b. A third and a forth branch appear at U_2 = 2.73 V and U_2 = 2.59 V, respectively, manifesting the transition into a period-3 (S^2L) state, and a period-4 (S^3L) state.

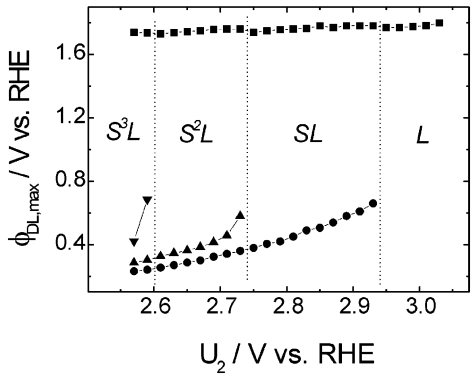

Figure 3. Bifurcation diagram showing $\phi_{DL,max}$ (see text) as a function of U_2 for the same experimental conditions as in Figure 1.

Two trends become apparent: First, the higher the period of the CV, the smaller is the range of anodic turning points, U_2, in which the respective cycle exists. At this point we note that in the experiments, U_2 was changed in steps of 20 mV. Thus, we cannot exclude that between two observed states more complicated concatenated states, in which the observed principle states alternate in a periodic or aperiodic fashion, exist in U_2 intervals smaller than 20 mV. For further discussion of this aspect, see section 3.2.

Second, along the lower $\phi_{DL,max}$ branches and differently from the upper one, $\phi_{DL,max}$ decreases with decreasing U_2. If $\phi_{DL,max}$ is smaller than a critical value, a new S cycle is born. This trend reflects the fact that a lower value of U_2 stabilizes the small hysteresis loop.

For a slightly larger H_2SO_4 concentration and thus a smaller uncompensated resistance but identical parameters otherwise, exclusively states with a larger number of S cycles than under the previous conditions were observed when decreasing U_2 in 10 mV steps from the period-1 L cycle. The low period states from the example discussed above are most likely squeezed to a small range of U_2 values close to the transition to the period-1 L cycle. Moreover, at this lower cell resistance the behavior was usually not strictly periodic; rather, in most cases the number of S cycles changed in an aperiodic manner around some mean value. Two examples of complex responses at this higher conductivity are reproduced in Figure 4. Figure 4a shows an S^5L state, which is, however, not strictly periodic as evident from the time trace of $\phi_{DL,max}$. In Figure 4b an aperiodic state is depicted, in which the number of S cycles between two L cycles varies between 5 and 7 in an apparently random manner.Upon lowering U_2 further, the average number of S cycles tended to increase, being 12 at U_2 = 2.63 V.

2.3. Discussion. The fact that a cyclic voltammogram does not retrace itself during every cycle of the applied voltage but after several cycles implies that the system has some kind of memory to the previous cycle. Such a memory effect arises if there is a process whose characteristic time is of the same order of magnitude as the cycling time and which interacts with at least one of the reaction steps or other processes that occur during a cyclic voltammogram. Hence, the key to understanding the complex voltammetric responses lies in identifying this process. Looking at Figure 2, it is apparent that while the system undergoes S cycles, the maximum current density and also the current density at any given value of U decreases from cycle to cycle whereas the activity is reestablished after an L cycle. This indicates that the process we are looking for affects the catalytic activity of the electrode with respect to hydrogen oxidation. The increase in the catalytic activity after an L cycle points to the

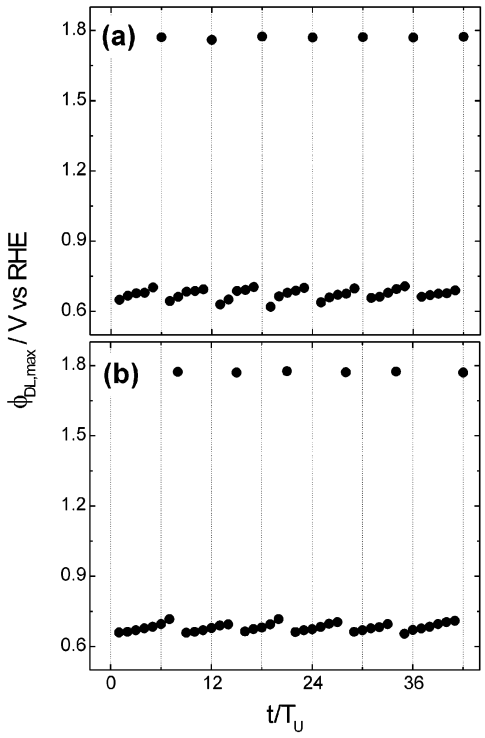

Figure 4. S^5L and aperiodic responses during cyclic voltammetry of H_2 oxidation on Pt in 1 mM H_2SO_4. Shown is the largest value of the true electrode potential $\phi_{DL,max}$ vs time. (Time is normalized to the period of a voltage cycle, T_u). Positive turning point: (a) $U_2 = 2.69$ V; (b) $U_2 = 2.70$V. Uncompensated cell resistance $R_\Omega = 360\ \Omega$. The remaining experimental parameters are identical to those in Figure 1.

fact that the essential interaction is through oxide formation or reduction, i.e., through reaction steps iv and v.

It is well established that Pt−oxide reduction causes a roughening of the Pt surface, due to place exchange process occurring during Pt oxidation. The latter occurs in addition to steps iv and v and can be formerly written as

$$\text{Pt}-\text{OH} \rightarrow \text{OH}-\text{Pt} \qquad \text{(vi)}$$

$$\text{Pt}-\text{O} \rightarrow \text{O}-\text{Pt} \qquad \text{(vii)}$$

Steps vi and vii are known to come into play after the (reversible) deposition of the first 15% of a monolayer of OH or O.[15−18] Therefore, further oxidation proceeds concomitantly to the place exchange process, and thus in an irreversible way. In our context, it is very important that the rough Pt surface resulting from the Pt−oxide reduction is known to relax back to its flat state in a rather reversible way; i.e., when the electrode is kept for a sufficient time negative to the potential region in which oxide formation occurs, the electrode surface flattens again.[14,19] These two processes, roughening of the surface and its subsequent relaxation, possess exactly the characteristics we are looking for. A rougher surface implies a larger surface area and thus a higher current. The healing or flattening of the electrode surface causes a subsequent deactivation. Furthermore, the relaxation is a slow process as shown in cyclic voltammetric experiments in N_2-saturated H_2SO_4, in which the charge under the hydrogen upd peaks decreased during several voltage scans if the electrode potential was kept sufficiently negative such that Pt−oxide did not form.[19]

As for the occurrence of high-order periodic voltammetric responses, the following question remains: If the positive turning point is so positive that Pt−oxide can form in one cycle, why does it not form in every cycle? In other words, why does

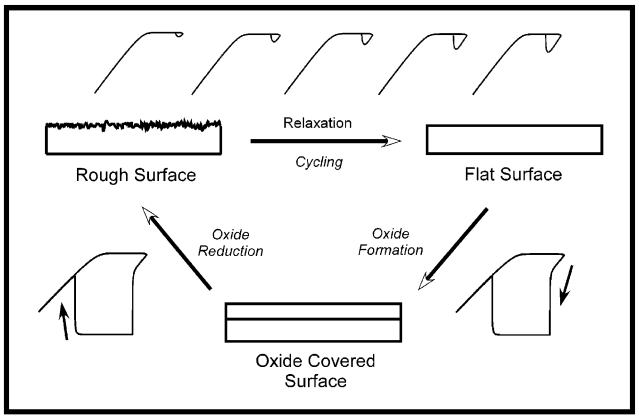

Figure 5. Illustration of the interplay between surface activity changes and ohmic drop through the electrolyte leading to the complex voltammetric behavior.

the rougher surface prevent the electrode from being oxidized again at the same value of the applied voltage in the next cycle? At this point, the electrolyte conductivity comes into play. Recall that the maximum true electrode potential, $\phi_{DL,max}$, increases from cycle to cycle while the system undergoes S cycles and ϕ_{DL} reaches a value of which the oxidation of the Pt surface sets in when finally an L cycle is initiated. Hence, it is the larger IR_Ω drop through the electrolyte that is associated with the more active surface and takes care that the electrode potential at the positive turning point of the applied voltage stays negative to Pt−oxide formation. Only when the relaxation of the surface toward a flat surface is sufficiently advanced and thus the current density has sufficiently decreased, becomes the electrode potential so positive that it enters a potential region at which the oxidation of the electrode sets in. The large hysteresis loop is then initiated by a self-enhancing feedback mechanism: Since the oxidized surface is inactive for hydrogen oxidation, the initial (hydr)oxide formation causes a decrease in current density. Owing to the smaller current density, the true electrode potential becomes more positive, and thus the oxide formation faster. In this way the true electrode potential is driven far into the oxide region. In other words, the oxidation of the Pt electrode leads to a negative differential resistance (NDR) in the stationary (and IR_Ω corrected) current potential curve. An NDR is well-known to give rise to the described self-enhancing feedback for a sufficiently large cell resistance. It is in fact the destabilizing process in most electrochemical systems that exhibit bistability or oscillations.[20−23]

The positive feedback is the more pronounced the higher the cell resistance R_Ω is: If the true electrode potential acquires a value at which oxide formation is about to start, a certain decrease of the current prompts all the more a positive electrode potential the larger R_Ω is. Consequently, also oxide formation is accelerated and thus I decreases more strongly. This trend offers a plausible interpretation of why we observe complex CVs with a large number of S cycles between two L cycles predominantly in the electrolyte with the higher conductivity.

In summary, the complex voltammetric responses are the result of the interplay between surface roughening owing to the reduction of Pt−oxide and the subsequent relaxation of the surface, on one hand, and the IR_Ω drop through the electrolyte coupled to a negative differential resistance, on the other hand. The scheme depicted in Figure 5 illustrates this mechanism.

3. Model and Simulations

3.1. The Model. The main ideas of the mechanism discussed above can be translated into a mathematical model consisting

of a set of ordinary differential equations. The variables of the model are the true electrode potential, ϕ_{DL}, the (hydr)oxide coverage of the electrode, θ, and the roughness of the electrode surface, r. The latter is defined as the ratio between the actual electrode area, A, and the electrode area of the relaxed (flat) surface, A_0; thus, $r \geq 1$.

The evolution equation for ϕ_{DL} is readily obtained from Kirchhoff's law applied to the equivalent circuit of an electrochemical cell (see for example refs 20−23) and reads

$$C_{sp}\frac{d\phi_{DL}}{dt} = -i_{reac} + \left(\frac{U - \phi_{DL}}{rA_0R_\Omega}\right) \quad (1)$$

where C_{sp} is the specific double layer capacitance (which is assumed to be constant), U the applied (and time-dependent) voltage, and R_Ω the uncompensated electrolyte resistance, i.e., the resistance between the WE and the RE. According to the above given definition of A_0 and r, rA_0 is the actual electrode area. The faradaic current density i_{reac} is composed of the hydrogen oxidation current density, and the current density due to the formation and reduction of Pt−oxide,

$$i_{reac} = -i_H(1 - 0.99\theta) - q_0\frac{d\theta}{dt}, \quad (1a)$$

where q_0 is the charge which flows if one monolayer oxide is deposited on or stripped from an electrode of 1 cm^2 in area. The hydrogen oxidation current density i_H $(1-0.99\theta)$ is assumed to instantaneously adjust to variations in ϕ_{DL} and θ. The factor 0.99 takes into account that the observed oxidation current was not identical zero even on an oxide covered electrode surface. For the sake of simplicity, the dependence of i_H on ϕ_{DL} on the bare Pt surface was modeled by the following equation

$$i_H = b_1 - \frac{b_2}{1 + \exp[b_3(\phi_{DL} - b_4)]}, \quad (1b)$$

whereby the constants b_1, b_2, b_3, and b_4 were obtained from a fit to experimental data. Their values are listed in Table 1.

Oxide formation and reduction was approximated by the Butler−Volmer-type equation

$$\frac{d\theta}{dt} = k_{ads}(1 - \theta)\exp[\alpha nf(\phi_{DL} - \phi_{DL,\theta=0.5})] - k_{des}\theta\exp[-(1 - \alpha)nf(\phi_{DL} - \phi_{DL,\theta=0.5})] \quad (2)$$

where k_{ads} and k_{des} represent the adsorption and desorption constants of oxide formation and dissolution, respectively. f stands for F/RT, whereby F, R, and T have their usual meanings. α is the transfer coefficient, and n represents the number of electrons transferred. $\phi_{DL,\theta=0.5}$ is the potential at which the electrode is half covered by oxide. Following Angestein-Kozlowska et al.,[24] the values of k_{ads} and k_{des} were chosen such that the peak separation of the oxidation and reduction current were close to the experimentally observed ones.

The "heart" of our model is the evolution of the surface roughness, r, with time, which was described by the following equation

$$\frac{dr}{dt} = K_r k_{des}\theta\exp[-(1 - \alpha)nf(\phi_{DL} - \phi_{DL,\theta=0.5})] - K_s(r - 1) \quad (3)$$

The first term in eq 3 models the roughening of the surface, which is assumed to be proportional to the desorption rate of oxide, K_r being a constant of proportionality. The flattening process is described by a simple, potential-independent relaxation of the rough to the smooth surface with the rate constant K_s.

TABLE 1: List of Symbols (with Their Meanings, Values Used in the Calculations, and Units)

symbol	meaning	(value) units
k_{ads}	adsorption constant	(0.1) s^{-1}
k_{des}	desorption constant	(0.05) s^{-1}
α	transfer coefficient	(0.5)
n	transferred electrons	(2)
θ	electrode coverage (normalized to the maximum electrode coverage)	
i_H	hydrogen current density	mA cm^{-2}
i_{reac}	faradaic current density	mA cm^{-2}
I	current	mA
q_0	charge that flows when 1 mL of oxide is formed on an electrode of 1 cm^2 [a]	(0.22) mC cm^{-2}
f	F/RT	(38.92) V^{-1}
C_{sp}	specific double layer capacitance	(0.02) mF cm^{-2}
R_Ω	uncompensated cell resistance	W
U	applied voltage	V
ϕ_{DL}	double layer potential	V
$\phi_{\theta=0.5}$	potential at which $\theta = 0.5$	(0.72) V
U_1	lower (negative) potential turning point	(0.27) V
U_2	upper (positive) potential turning point	V
ν	scan rate	(0.1) V s^{-1}
A_r	real electrode area	cm^2
A_0	apparent (geometric) electrode area	(1) cm^2
r	electrode roughness ($=A_r/A_0$)	
t	time	s
T_u	period of one voltammetric cycle ($=2(U_2 - U_1)/\nu$)	s
K_r	roughening constant	(0.01)
K_s	relaxation or smoothing constant	(0.05) s^{-1}
b_1	constant in eq 1b	(6) mA cm^{-2}
b_4	constant in eq 1b	(2073) mA cm^{-2}
b_3	constant in eq 1b	(22.66) V^{-1}
b_4	constant in eq 1b	(0.26874) V

[a] We assume that per Pt atom two electrons are involved in the oxidation process (see eq 3 and the value for n in this table). Thus, the value chosen for q_0 implies that the maximum oxide coverage which completely inhibits hydrogen oxidation is 0.5. We confirmed that also for a maximum oxide coverage of 1, and thus $q_0 = 440$ mC cm^{-2}, the same qualitative trend as reported here occurs. However, the absolute values of U at which a particular behavior is found are shifted toward larger values; in addition the bifurcation fine structure might be slightly altered.

Finally, the periodic cycling of the externally applied voltage U between two limit points, U_1 and U_2, can formerly be written as

$$\frac{dU}{dt} = \begin{cases} \nu, U_1 \rightarrow U_2 \\ -\nu, U_2 \rightarrow U_1 \end{cases} \quad (4)$$

where ν is the scan rate, $U_1 \rightarrow U_2$ symbolizes that $dU/dt > 0$ and $U_1 \leq U < U_2$. Accordingly, $U_2 \rightarrow U_1$ means that $dU/dt < 0$ and $U_1 < U \leq U_2$.

The time integration of eqs 1−4 was performed with the Livermore solver for ordinary differential equations (lsode) invoking the mode for stiff systems.[25] All parameters, which were not changed in the simulation, are compiled in Table 1. With the exception of K_r and K_S, they were either known from literature or fitted to independent experiments.

3.2. Simulations and Discussion. Integrating eqs 1−4 reveals that this set of equations possesses indeed high-order periodic and aperiodic solutions, which bare all the properties of the experimentally observed complex cyclic voltammetric responses for realistic values for the parameters. Note, however, that we

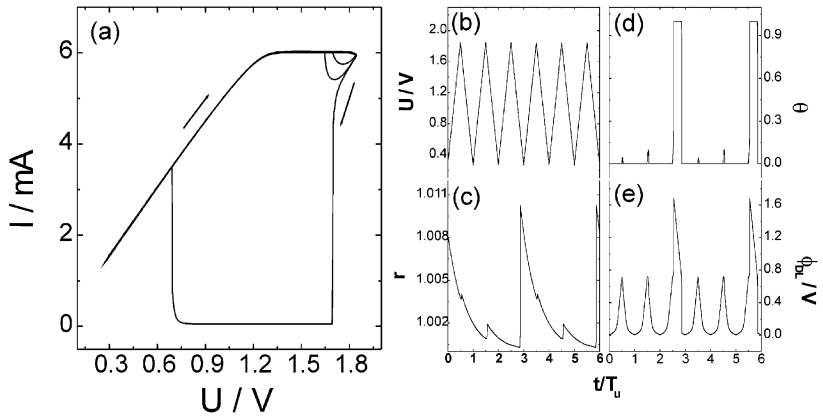

Figure 6. (a) Calculated period-3 (S^2L) voltammetric response and corresponding time series of (b) U, (c) r, (d) θ, and (e) ϕ_{DL}. T_u period of the cycling voltage. $R_\Omega = 190\ \Omega$ and $U_2 = 1.8445$ V; the remaining parameters are given in Table 1.

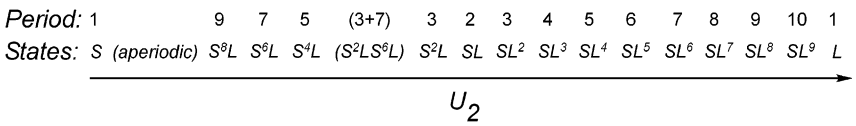

Figure 7. Different dynamic states observed upon decreasing U_2 from the L state. $R_\Omega = 190\ \Omega$, the remaining parameters and the numerical values for U_2 at which the respective states exited are given in Tables 1 and 2, respectively.

used in the calculations values for the cell resistance that were smaller than those in the experiments since for realistic values the problem was so stiff that it was difficult to handle numerically. A calculated period three solution representing an S^2L state is shown in Figure 6.

In Figure 6a, the voltammetric response is depicted, whereas parts b−e of Figure show the temporal change of the externally applied voltage, the surface roughness, the oxide coverage of the electrode, and the true electrode potential, respectively. Clearly, the calculated cyclic voltammogram exhibits the same basic features as the experimentally obtained period three response shown in Figure 1c, namely a periodic behavior which is composed of two small hysteresis loops followed by a large hysteresis loop. Furthermore, for potentials close to U_2 the current density is smaller in the second S cycle than in the first one. This feature is particularly pronounced on the negative scan in both experiment and simulations. However, on the positive voltage scan it is more pronounced in the experiments than in the simulations. This small discrepancy probably results from the value chosen for the constants determining surface roughening and flattening, K_r and K_s. Since eq 3 represents only a crude approximation to the roughening process, these constants, which are not available from the literature, were only roughly adjusted to the observed time scales and no attempt was made to quantitatively match the experimental behavior. Two other discrepancies between the experimental and simulated CVs are apparent: First, in the experiments the mass transport limited current region exhibits a small decrease when going to positive potentials, which is not the case in the simulation. This is a result of the chosen function (eq 1b) used to model the hydrogen current, where the fit to the experimental data exhibited a small discrepancy in this potential region. The second dissimilarity is the residual current after the oxide formation, which is seen in the experiment but is not reproduced in the calculations. As discussed above, this current is due to the oxygen evolution reaction. For the sake of simplicity, the latter was not included in our model.

To obtain a better picture of the dynamics, it is instructive to follow how the variables change in the course of this period three response (Figure 6, parts b−d). As is apparent from Figure 6c, the surface roughness increases jumplike when going from the oxide covered to the bare Pt electrode and essentially relaxes during the three subsequent voltage cycles to its original value. This relaxation is slightly disturbed when the minor oxide coverage, which forms during the S cycles (cf. Figure 6d), is reduced. Thus, the relaxation phase is modulated with the cycling period. It is remarkable that the changes in the surface roughness are only on the order of 1%, which means that minor changes in the electrode area that are very hard to detect experimentally suffice to induce the complex voltammetric response. Parts d and e of Figure 6, in which the changes of the oxide coverage and the true electrode potential are shown, confirm the picture we have developed above, namely that an increasing oxide coverage goes along with an increasing value of ϕ_{DL} (though the latter one is not as pronounced as in the experiments and is not evident in the scale of the figure).

Varying U_2 while keeping constant all other parameters used to produce Figure 6 exhibits a large variety of complex cyclic voltammetric responses, including aperiodic states as well as responses where the number of S cycles between two L cycles alternates. An overview of the obtained dynamics is depicted in Figure 7. Note that in this figure the abscissa is strongly nonlinear since some of the states existed only in tiny parameter intervals whereas other states occurred in large regions of U_2. Representative values of U_2 for which the respective behavior was observed are compiled in Table 2.

Figure 7 exhibits some general features and trends that are independent of the special parameter sets used in the calculations. First, the U_2 range of complex responses is encircled by period-1 CVs of the small hysteresis-type to the low-potential end, and period-1 CVs with large hysteresis loops at the high potential end. When U_2 is increased from the period-1 S cycle, the S cycles are at first only seldom interrupted by an L cycle and later more and more often until L and S cycles take turn in the period-2 SL state. Upon further increasing U_2, two S cycles are now separated by several L cycles, whereby the number of L cycles increases until the threshold is reached at which the period-1 L response exists.

Looking only at the right part of the diagram shown in Figure 7 one could get the impression that upon decreasing U_2 only states SL^n exist whereby n decreases from ∞ to 1 as U_2 decreases. A further decrease of U_2 would then naturally reverse

TABLE 2: Typical U_2 Values for the States Described in Figure 7

U_2/V	observed states
<1.84426	P1−*S*
1.844293	(aperiodic)
1.844294	P9−S^8L
1.844295	P7−S^6L
1.844297	P5−S^4L
1.844303	(S^2LS^6L)
1.844304	P3−S^2L
1.844900	P2−*SL*
1.848500	P3−SL^2
1.848900	P4−SL^3
1.849000	P5−SL^4
1.849010	P6−SL^5
1.849020	P7−SL^6
1.849022	P8−SL^7
1.849025	P9−SL^8
1.849026	P10−SL^9
>1.849035	P1−*L*

this sequence, producing S^nL states with n increasing from 1 to ∞. However, as apparent from the left part of Figure 7, this picture is too simple. Instead, in some calculations between two such base states, concatenated states which partly existed only in tiny parameter intervals were detected. For the present set of parameters, such a state is, e.g., the S^2LS^6L state. Furthermore, aperiodic states, in which the number of *S* states between two *L* states alternated in an apparently random manner around an average number, similar to observations in the second set of experiments at higher conductivity, were found (cf. Figure 4b). These observations suggest that the complete bifurcation diagram is likewise complicated as those found for so-called mixed-mode oscillations.[26,35]

The existence of the aperiodic and concatenated states also evidences that the complex responses cannot be explained by a linear superposition of two time scales, the cycling period and the relaxation time. Instead, the dynamics is the result of the coupling between the forcing period of *U* and nonlinearities in the evolution equations. As discussed above, at low ionic strength the decrease of current density owing to oxide formation gives rise to a self-enhancing ("autocatalytic") growth of the (true) electrode potential, which causes the system to be bistable under stationary conditions: In a certain range of *U*, the system can either be in an "active" state where hydrogen oxidation proceeds on the bare Pt surface with a high rate or in a passive state, in which the electrode surface is covered by oxide and the current density is low. Thus, from a dynamical point of view we are dealing with a periodically forced bistable system.

We did some (though not extensive) tests whether the complex responses also exist if it is assumed that Pt−oxide does not inhibit the reaction, i.e., with eqs 1−4 where in eq 1a the term $(1 - 0.99\theta)$ was omitted. This removes the positive feedback loop in the system. In the simulations only period-1 CVs were obtained which points to the fact that the autocatalysis is indeed necessary for the occurrence of the complex, nonlinear behavior.

In calculations with a smaller cell resistance, S^nL periods with n larger than in Figure 7 were obtained easily, whereas the highest SL^n states of the above simulations were not detected. Besides, the relative ΔU_2 interval[36] in which S^nL states existed was larger at the higher conductivity. This is the same trend which was observed in the experiments (cf. Figures 1 and 4) and which becomes plausible when considering the fact that the positive feedback is weaker at higher conductivity (s.a.). In addition, in the simulations with a higher conductivity complex dynamic behavior existed which was only composed of *S* cycles for values of U_2 that were lower than the one at which the first *L* cycle appeared. In Figure 8, a bifurcation diagram is shown in which the maximum values of θ during each period of the voltage cycling is plotted vs U_2. Note that θ_{max} is considerably smaller than 1 throughout whereas it would be close to 1 in an *L* cycle. The bifurcation diagram is typical for a period-doubling cascade to chaos.[29,30] The next maximum map depicted in Figure 9 has (with the exception of one point) an unimodal shape as typical for chaos arising through the Feigenbaum scenario. This behavior is a further manifestation that nonlinearities in the evolution laws are decisive for the complex voltammetric responses. Furthermore, they demonstrate that even the exclusive formation and dissolution of oxide in the submonolayer region which bring about only a minor roughening of the surface suffice to induce complex behavior.

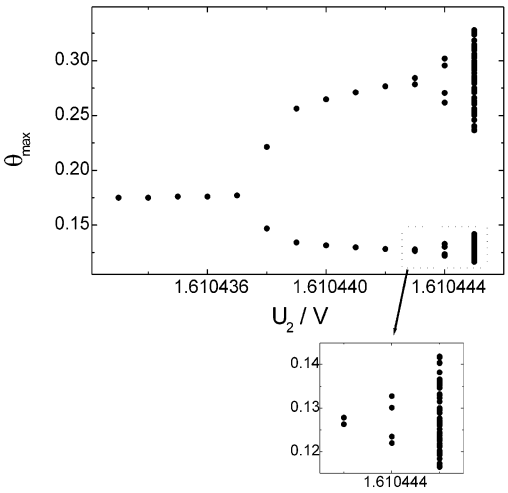

Figure 8. Calculated bifurcation diagram for $R_\Omega = 150\ \Omega$. The remaining parameters are given in Table 1.

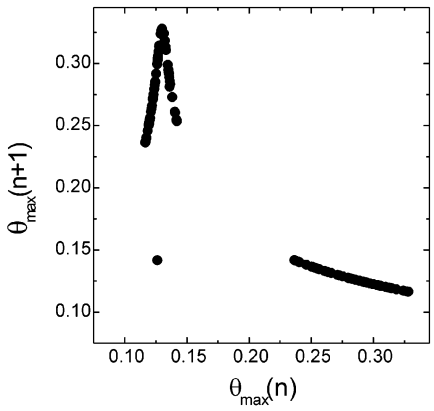

Figure 9. Next maximum map for the data shown in Figure 8 at $U_2 = 1.610445$ V.

4. General Discussion

According to our considerations above, the essential "ingredients" necessary to cause higher periodic and aperiodic cyclic voltammograms are as follows: (a) a faradaic reaction that is inhibited by oxide formation on the electrode and thus generates an NDR in the polarization curve at positive potentials; (b) a nonnegligible ohmic drop through the electrolyte which together with the NDR gives rise to a positive feedback in the electrode potential; (c) a roughening of the electrode surface due to oxide reduction and its subsequent relaxation to a flat surface, whereby

the relaxation has to occur on a time scale which is at least of the order of the voltage cycling period.

These conditions are fulfilled by different noble metal electrodes, whereby Pt and Pd are probably the most important ones, and a large variety of oxidation reactions, in particular the electrocatalytic oxidation of small organic molecules such as formic acid, aldehydes, or alcohols. This suggests that also the large variety of complex cyclic voltammograms reported by Schell and coworkers[3−10] are brought about by this principle mechanism. One criterion, which these results should then satisfy, is that the complex responses should disappear when the ohmic drop is negligible. In ref 10 Zdraveski et al. investigate the impact of the uncompensated resistance in two sets of experiments. In one set, the cell resistance is changed by varying the position of the RE, in the other one by variation of the sodium hydroxide concentration. Starting from a period-2 response, in both sets of experiments a decrease in the uncompensated cell resistance, R_Ω, lead eventually to period-1 behavior. Thus, the authors concluded "R_Ω cannot be eliminated from playing a role in the cause of instability...",[10] which is in accordance with our conjecture.

As mentioned in the Introduction, complex voltammetric responses were also observed during Cu dissolution in acidic solution.[11] It seems to be conceivable that also here the same principle mechanism is operative: Upon increase of the electrode potential the "active" dissolution of Cu is hindered due to the passivation of the Cu surface which is caused by its oxidation. Hence the polarization curve possesses an NDR. Furthermore, it appears to be likely that reduction of the oxide goes also along with roughening and subsequent healing of the surface. This example demonstrates how manifold the reactions might be in which roughening/relaxation of the electrode surface coupled to an NDR causes dynamic instabilities of CVs.

So far we stressed the basic features that give rise to complex cyclic voltammetric responses. However, different bifurcation scenarios between the period-1 *S* and *L* cycles as a function of U_2 were observed in different reactions and also for different experimental condition in one reaction (see, e.g., ref 9). In view of this manifold of different dynamic states observed, it is natural to ask for the causes of these differences. At this point, it is important to note that the detailed route through the U_2 window of complex response depends sensitively not only on the value of parameters that do not affect (at least in zeroth order) the electrode kinetics (such as the conductivity, where the correct trend could be reproduced in the simulations) but also on details of the reaction mechanism and thus on the specific electrochemical reaction under investigation. Furthermore, the relaxation process will be in general potential dependent and can be altered by adsorbates. E.g., it is known that Cl^- ions enhance the mobility of adatoms on gold surface and lead to chemical annealing,[31−34] other adsorbed species will reduce the rate of relaxation. All these aspect will determine the intricate bifurcation fine structure. Thus, our explanation of the occurrence of high-order periodic or aperiodic CVs should not be understood as being exhaustive. Instead, it gives a minimum skeleton, which can give rise to complex voltammetric responses of the desired type and is the primary reason for dynamic instabilities in cyclic voltammograms in many electrochemical reactions.

Besides these aspects, one should be aware of another assumption that we have so far implicitly made, namely that spatial variations can be neglected. However, it is known that oxide formation proceeds through a nucleation and growth mechanism. In fact, we were able to measure the potential distribution along our ring electrode during cyclic voltammetry (for the experimental setup, see ref 13) and observed that the transition from the free Pt electrode to Pt−oxides occurs on our rather large electrode even on a mm scale never completely homogeneously. In some voltage cycles the entire electrode became even never completely covered by oxide. Instead, an oxide area expanded along the ring until the electrode was approximately half covered by it. Successively, it shrank again. In the cyclic voltammogram, these (rather seldom) occurrences manifested itself in current−potential curves, in which the current decreased to approximately half of its highest value, the entire cycle resembling neither a typical *S* nor a typical *L* cycle. It is remarkable that also in the studies by Schell and co-workers such intermediate cycles are sporadically reported (see, e.g., Figure 1b in ref 10). Hence, except for very small electrodes, the dynamic behavior is a spatiotemporal phenomenon, the fine structure of the bifurcations being captured only when taking also the spatial coordinate into account.

5. Conclusions

The occurrence of complex cyclic voltammograms implies that there is a slow process with a characteristic time on the order of the period of the cycling voltage that interacts with the remaining electrochemical steps. We identified the relaxation of a rough surface, which is generated when an oxidized electrode surface is reduced, to a smooth surface as such a process. Surface roughening and healing is most likely an essential step in all of the so far reported complex voltammetric responses.

Further essential features are (a) that an oxidation reaction proceeds more slowly on the oxidized than on the bare electrode surface, i.e., that the polarization curve possesses a region of negative differential resistance and (b) that there is a nonnegligible ohmic potential drop through the electrolyte. The latter is often the case even for small cell resistances since the reaction rate easily takes on considerable values at potential values close to the onset of oxide formation.

The derived conditions are general and hold under many experimental situations, suggesting that complex voltammetric responses are no exotic phenomena but exist for a large variety of electrode reactions and electrode materials.

Acknowledgment. The authors would like to thank F. Plenge and Y.-J. Li for fruitful discussions. H.V. thanks the MPG for a Ph.D. scholarship and the ESF/Reactor Program for travel support.

References and Notes

(1) Bard, A. J.; Faulkner, L. R. *Electrochemical Methods: Fundamentalas and Applications*; Wiley: New York, 1980.
(2) Hamann, C. H.; Hamnett, A.; Vielstich, W. *Electrochemistry*; 1998, Wiley/VCH: Weinheim, Germany, 1998.
(3) Parida, G. R.; Schell, M. *J. Phys. Chem.* **1991**, *95*, 2356.
(4) Schell, M.; Cai, X. R. *J. Chem. Soc., Faraday Trans.* **1991**, *87*, 2255.
(5) Cai, X. R.; Schell, M. *Electrochim. Acta* **1992**, *37*, 673.
(6) Schell, M.; Cai, X. R. *Electrochim. Acta* **1993**, *38*, 519.
(7) Xu, Y. H.; Amini, A.; Schell, M. *J. Phys. Chem.* **1994**, *98*, 12759.
(8) Schell, M.; Xu, Y. H.; Amini, A. *J. Phys. Chem.* **1994**, *98*, 12768.
(9) Xu, Y. H.; Amini, A.; Schell, M. *J. Electroanal. Chem.* **1995**, *398*, 95.
(10) Zdraveski, Z.; Xu, Y. H.; Amini, A.; Schell, M. *J. Chem. Soc., Faraday Trans.* **1996**, *92*, 395.
(11) Dolata, M.; Kawczynski, A. L. *Pol. J. Chem.* **2000**, *74*, 1625.
(12) Varela, H.; Krischer, K. *Catal. Today* **2001**, *70*, 411.
(13) Grauel, P.; Krischer, K. *Phys. Chem. Chem. Phys.* **2001**, *3*, 2497.
(14) Tremiliosi-Filho, G.; Jerkiewicz, G.; Conway, B. E. *Langmuir* **1992**, *8*, 658.
(15) Conway, B. E.; Kozlowska, H. A.; Sharp, W. B. A. *J. Electroanal. Chem.* **1973**, *43*, 9.

(16) Conway, B. E. *Prog. Surf. Sci.* **1995**, *49*, 331.
(17) Conway, B. E. *Prog. Surf. Sci.* **1984**, *16*, 1.
(18) Conway, B. E. *J. Electroanal. Chem.* **2002**, *524*, 4.
(19) Hoare, J. P. *Electrochim. Acta* **1982**, *27*, 1751.
(20) Koper, M. T. M. In *Oscillations and complex dynamical bifurcations*; Advances in Chemical Physics 92; Prigogine, I., Rice, S. A., Eds.; Wiley: New York, 1996; p 161.
(21) Krischer, K. Principles of spatial and temporal pattern formation in electrochemical systems. In *Modern Aspects of Electrochemistry*; Conway, B. E., Bockris, J. O. M., White, R., Eds.; Kluwer Academic/Plenum: New York, 1999, p 1.
(22) Krischer, K. *J. Electroanal. Chem.* **2001**, *501*, 1.
(23) Krischer, K.; Mazouz, N.; Grauel, P. *Angew. Chem., Int. Ed.* **2001**, *40*, 851.
(24) Angestein-Kozlowska, H.; Conway, B. E.; Klinger, J. *J. Electroanal. Chem.* **1977**, *75*, 45.
(25) Hindmarsch, A. C. *ACM-SIGNUM Newsl.* **1980**, *15*, 10.
(26) Ringland, J.; Issa, N.; Schell, M. *Phys. Rev. A* **1990**, *41*, 4223.
(27) Albahadily, F. N.; Ringland, J.; Schell, M. *J. Chem. Phys.* **1989**, *90*, 813.
(28) Krischer, K.; Lubke, M.; Eiswirth, M.; Wolf, W.; Hudson, J. L.; Ertl, G. *Physica D* **1993**, *62*, 123.
(29) Berge, P.; Pomeau, Y.; Vidal, C. *Order within chaos: towards a deterministic approach to turbulence*; Wiley: New York, 1986.
(30) Schuster, H. G. *Deterministic chaos: an introduction*; VCH: Weinheim: Germany, 1988.
(31) Kolb, D. M. *Prog. Surf. Sci.* **1996**, *51*, 109.
(32) Giesen, M.; Kolb, D. M. *Surf. Sci.* **2000**, *468*, 149.
(33) Cuesta, A.; Kolb, D. M. *Surf. Sci.* **2000**, *465*, 310.
(34) Kolb, D. M. *Angew. Chem., Int. Ed.* **2001**, *40*, 1162.
(35) Mixed-mode oscillations are periodic or aperiodic oscillations which are composed of different numbers of small and large amplitude oscillations.[20,27,28]
(36) I.e., (U_2 at the border to the S^1 response $-$ U_2 in the middle of the interval in which *SL* cycles exist) normalized to the total U_2 interval in which complex CVs were detected.